European Journal of Radiology 118 (2019) 215–222

Contents lists available at ScienceDirect

European Journal of Radiology

journal homepage: www.elsevier.com/locate/ejrad

Research article

Value of spectral detector computed tomography for assessment of pancreatic lesions

Nada El Kayal[a,b,1], Simon Lennartz[a,d,1], Sandra Ekdawi[c], Jasmin Holz[a], Karin Slebocki[a], Stefan Haneder[a], Christian Wybranski[a], Ahmed Mohallel[b], Mohamed Eid[b], Holger Grüll[c], Thorsten Persigehl[a], Jan Borggrefe[a], David Maintz[a], Carola Heneweer[a,*]

[a] University of Cologne, Faculty of Medicine and University Hospital Cologne, Department of Diagnostic and Interventional Radiology, Cologne, Germany
[b] Department of Diagnostic and Interventional Radiology, Alexandria University, Faculty of Medicine, Alexandria, Egypt
[c] Experimental Imaging and Image-Guided Therapy, Institute of Diagnostic and Interventional Radiology, University Hospital of Cologne, Cologne, Germany
[d] Else Kröner Forschungskolleg Clonal Evolution in Cancer, University Hospital Cologne, Cologne, Germany

ARTICLE INFO

Keywords:
Dual energy computed tomography
Neoplasm staging
Pancreatic carcinoma
Pancreas

ABSTRACT

Purpose: Dual energy CT (DECT) can contribute to the diagnosis of benign and malignant pancreatic lesions. This study examined whether a novel, detector-based spectral CT scanner (SDCT) may improve subjective assessment of different types of pancreatic lesions and if various quantitative maps may improve lesion contrast and differentiation.

Materials and methods: 61 consecutive patients who underwent clinical, contrast-agent enhanced, abdominal SDCT scans and showed pancreatic lesions of different origins were included. Subjective image analysis was performed by two readers who assessed image quality, lesion conspicuity and diagnostic confidence on 5-point Likert scales for conventional polyenergetic reconstructions (polyE), virtual monoenergetic images (monoE), virtual non-contrast images, iodine density, iodine overlay, and Z effective (Z_{eff}) maps. Two readers acquired quantitative values from these maps ROI-based from which contrast-to-noise and lesion-to-parenchyma ratios were calculated.

Results: MonoE images at low keV levels yielded highest Likert scores regarding lesion conspicuity and reader confidence; iodine overlays facilitated lesion delineation. Inter-observer agreement ranged between substantial and excellent (kappa values 0.73-0.81). Contrast-to-noise-ratios for low keV monoE images were significantly higher, compared to polyE images (e.g. monoE 40 keV $p < 0.0001$). Marked overlap between PDAC and miscellaneous non-PDAC lesions was present in various spectral reconstructions.

Conclusions: In line with previous studies, monoE images at low keV levels and iodine overlay maps facilitated subjective lesion delineation which was substantiated by the quantitative analysis. Hence, spectral detector CT improves pancreatic lesion conspicuity, while its value for lesion differentiation needs to be further evaluated in larger study cohorts.

1. Introduction

Pancreatic ductal adenocarcinoma (PDAC) remains a fatal diagnosis in the majority of cases and represents the fourth leading cause of cancer-related deaths in the United States [1]. Surgical resection constitutes the only means that can lead to prolongation of life [2]. However, most patients fail to qualify for surgery, as they present with locally advanced or even metastasized tumors at initial diagnosis [3]. Nonetheless, an increasing number of studies indicates that a subgroup of patients may benefit from resection despite having been previously classified as irresectable—a category termed 'borderline resectable pancreatic cancer [4–6]. For these lesions, accurate visualization of the tumors is key, especially pertaining to delineation of vascular invasion. In this process, multiphasic multidetector single energy computed tomography (SECT) plays a major role [2,4,7–9]. However, early detection as well as determination of the extent of tissue infiltration remain a

Abbreviations: CI, Conventional CT imaging/images; CNR, Contrast-to-noise ratio; HU, Hounsfield Unit; ID, Iodine density; IO, Iodine overlay; MonoE, Virtual monoenergetic images; PDAC, Pancreatic ductal adenocarcinoma; SD, Standard deviation; SDCT, Spectral-detector CT; SECT, Single energy CT; Zeff, Z effective maps

* Corresponding author at: Institute for Diagnostic and Interventional Radiology, University Hospital of Cologne, Kerpener Str. 62, 50937 Köln, Germany.
E-mail address: carola.heneweer@uk-koeln.de (C. Heneweer).

[1] Authors contributed equally.

https://doi.org/10.1016/j.ejrad.2019.07.016
Received 15 February 2019; Received in revised form 8 July 2019; Accepted 15 July 2019

task difficult to comply with [3]. Another challenge of the CT-based diagnosis of pancreatic tumors are small lesions or tumors that appear nearly isodense to the surrounding pancreatic tissue [3,10,11]. As a considerable number of pancreatic lesions of unclear etiology are discovered incidentally during imaging performed for unrelated medical indications [12–15], accurate discrimination of PDAC from lesions of other origin would influence the consecutive clinical pathway substantially.

Dual-energy computed tomography (DECT) scanners acquire one high- and one low-energy dataset of the polyenergetic X-ray spectrum. Aside from reconstruction of polyE images, this allows for decomposition of the acquired datasets facilitating reconstruction of additional spectral series. Among these, iodine density (ID) maps are material-specific images in which voxels reflect the iodine concentration (mg/mL) of the displayed tissue [16]. The ID maps can be color-coded and fused with polyE images, generating so-called iodine overlay (IO) images. Conversely, virtual non-contrast (VNC) images represent approximations of contrast-enhanced images in which all iodine-related image information was removed [17]. Virtual monoenergetic (monoE) images approximate how the result of an acquisition with a monoenergetic X-ray beam would appear (40–200 keV) [18]. Z effective (Zeff) maps display the atomic numbers of the scan volume in a color-coded manner [17].

Over the past several years, DECT scanners have been marketed with different technical solutions using modifications of the X-ray tube (i.e., two tubes with different energies, or one tube with rapid switching between two energy levels) [19,20] and have proven to enhance both reader confidence and image quality of different pancreatic lesions [21,22]. In contrast, the spectral detector CT (SDCT) used in this study (IQon® Spectral CT, Philips Healthcare, Amsterdam, The Netherlands) is the first DECT based on the spectral separation of high and low energies on the detector level. Using SDCT, high-energy photons are simultaneously detected within the outer layer of the detector, whereas low-energy photons are recorded within the inner layer, resulting in the acquisition of retrospectively accessible spectral information with every scan [23]. Additionally, the spectral datasets are spatially and temporally registreted at full field-of-view without radiation dose penalty [24–26].

DECT holds the potential to improve lesion characterization and therapy monitoring in oncologic imaging [24,27], provided that the calculated spectral parameters add substantial value, not only for subjective lesion detection but also for quantitative differentiation. The current study evaluates the determination of such parameters and the possible value they may add to visual and quantitative assessment of pancreatic lesions.

2. Materials and methods

2.1. Study population

The institutional review board approved this study, waiving written informed consent due to its retrospective nature. Using the radiological information system, a search for patients matching the following criteria was executed: a) received portal-venous phase SDCT of the abdomen between June 2016 and February 2017, b) pancreatic lesion of any kind was mentioned in the radiological report, and c) age was > 18 years.

2.2. Lesion annotation

To validate lesion type stated within the radiological report, the respective pancreatic lesions of the initially identified patients were correlated with a reference standard. For that purpose, either histopathological confirmation (n = 26 patients), magnetic resonance imaging/endoscopic ultrasound correlation (n = 7 patients) or follow-up CT (n = 32 patients) were used. All 17 cases of PDAC were histopathologically confirmed. All other lesions were assigned to four groups (cyst, hypodense, isodense, hyperdense) based on their density values on polyE images.

2.3. Image acquisition

All patients were scanned on a clinical SDCT scanner (IQon, Philips Healthcare, Best, The Netherlands). The patients were scanned in cranio-caudal direction while remaining in a supine position during inspirational breath-hold.

After intravenous administration of a body weight-adapted volume of non-ionic, iodinated contrast agent (Accupaque 350 mg/mL, GE Healthcare; Little Chalfort, UK) via a peripheral vein with a mean flow of 3.5 mL/s followed by a 30 mL saline chaser, the scans were started with a delay of 50 s after passing the predetermined threshold of 150 HU within the abdominal aorta (activated bolus tracking). Tube current modulation was activated by default (DoseRight 3D-DOM; Philips Healthcare, Best, The Netherlands). Mean CTDI for the venous scan was 10.7 ± 3.5. The following parameters were used: tube voltage 120 kVp, collimation 64 × 0.625 mm; rotation time 0.5 s; pitch 0.671.

2.4. Image reconstruction and post-processing

Reconstructions of polyE, monoE at 40–200 keV, VNC, ID and Z_{eff} series as well as IO images were performed on a dedicated vendor console (IntelliSpace Portal 9.0, Philips Healthcare, Best, The Netherlands). All further analyses were carried out on the same console. Only images in portal-venous phase were evaluated. As in clinical routine, conventional polyE images were reconstructed using iDose 4 (level 3). For reconstruction of all spectral parameters (monoE, VNC, ID, Z_{eff}, IO), a dedicated spectral reconstruction algorithm (Kernel B, strength level 3) was used, which is comparable to hybrid-iterative reconstruction methods in the conventional polyE images. For that purpose, a slice thickness of 2 mm was predetermined.

2.5. Subjective image analysis

To assess pancreatic lesions subjectively, two radiologists with 2 and 7 years of experience, respectively, reviewed polyE, $monoE_{40}$, ID, IO and Z_{eff} reconstructions and evaluated the following criteria using a five-point Likert scale: general image quality (1: severe distortion; 2: poor quality; 3: fair but compromised quality; 4: good quality; 5: excellent quality), lesion conspicuity (1: barely perceived; 2: subtly visualized; 3: fairly detectable; 4: definitely detected; 5: strikingly evident/easily spotted), diagnostic confidence (1: definitely no lesion; 2: probably no lesion; 3: indeterminate; 4: probably a lesion; 5: definitely a lesion).

2.6. Objective image analysis

Quantitative analysis was performed by two experienced radiologists independently. Both reviewers placed circular regions of interest (ROIs) within the following predefined regions: pancreatic lesion, healthy pancreatic parenchyma, celiac trunc, psoas major muscle, and retroperitoneal fat. Contrast-to-noise ratio (CNR) was calculated with the following formula:

$$CNR = (HU_{pancreas} - HU_{lesion})/SD_{fat}$$

If more than one pancreatic lesion was detected, ROIs were placed in every lesion and the respective slice positions were reported. Necrotic areas were excluded. Sizes of the ROIs were determined in such a way that a maximum area of the respective lesion was covered. Initial ROI placement was performed in the polyE images. Subsequently, ROIs were copied to the following spectral reconstructions so that position and size of the ROIs remained constant: $monoE_{40-}$

$_{200keV}$, ID, Z_{eff}. Mean and standard deviation (SD) for every ROI and reconstruction (polyE, $monoE_{40\text{-}200keV}$, ID, Z_{eff}) as well as the long axis diameter were recorded. Values were normalized to respective iodine contents in the celiac trunc in a separate approach to correct for random differences in contrast agent injections and inflow. Additionally, lesion-to-parenchyma ratios were calculated (l-p-ratio).

2.7. Statistical analysis

Statistical data analysis was performed with a standard statistics software (JMP 11, SAS, Cary, USA). Inter-reader agreement for the subjective assessment was calculated with quadratic weighted Cohen's kappa coefficients (κ), with values of ≥ 0.81 indicating excellent, 0.61–0.80 substantial, 0.41–0.60 moderate, 0.21–0.40 fair, and ≤ 0.20 poor agreement. Paired Wilcoxon-Mann-Whitney tests were performed to compare the subjective ratings, and to determine the potential of several parameters to discriminate different pancreatic lesions from each other. Statistical significance was defined as $p \leq 0.05$.

3. Results

3.1. Lesion characteristics

61 patients with 65 pancreatic lesions of various kinds were identified (Table 1). All PDAC were histopathologically confirmed, and allocated to a separate group irrespectable of their appearance on the polyE images. All remaining lesions were annotated to four other groups (cyst, hypodense, isodense, hyperdense) based on their density values obtained from polyE images (Table 2). Regarding lesion size, cystic (16.5 ± 12.1 mm) and hypodense lesions (20.4 ± 7.8 mm) were significantly smaller than PDAC (32.3 ± 17.7 mm; $p = 0.0008$ and $p = 0.0038$, respectively) while the sizes of isoattenuating and hyperdense lesions were comparable ($p = 0.12$ and $p = 0.13$, respectively). However, all lesions showed a considerable overlap regarding their sizes. Inter-reader agreement regarding size measurements was good ($R^2 = 0.85$).

3.2. Subjective analysis

Image quality was rated excellent overall (Fig. 1A). Lesion conspicuity was significantly higher on $monoE_{40}$, ID and IO reconstructions compared to polyE images, and lesions could be defined significantly better on all other reconstructions compared to Z_{eff} maps (Fig. 1B, Fig. 2, Table 3). No significant difference in lesion conspicuity could be found when comparing $monoE_{40}$, ID maps and IO images. Statistical analysis of reader confidence revealed the same results as for lesion conspicuity with one exception: comparison of polyE with ID maps did not reach statistical significance, and showed only a trend towards a higher reader confidence using ID maps compared to polyE images (Fig. 1C, Table 3). Inter-observer agreement ranged between substantial

Table 1
List of included pancreatic lesions sorted by type.

Diagnosis	number
Pancreatic ductal adenocarcinoma	17
Cyst	11
Intraductal papillary mucinous neoplasm	9
mucinous cystic neoplasm	1
neuroendocrine tumor	7
LymphomA	2
MetASTASIS	9
(1 colorectal, 1 leimyosarcoma, 1 ovary, 1 melanoma, 5 Renal)	
Chronic pancreatitis	1
Scar	2
Unknown	6
	65

Table 2
Image-based definition criteria of different lesion groups. polyE: polyenergetic reconstruction.

Group	Number	Definition (based on conventional polyE)
CYSTIC LESION	17	< 20 HU
IsoATTENUATING LESION	4	Pancreas density +/- 15 %
HyperATTENUATING LESION	9	> 115 % pancreas density
HypoATTENUATING LESION	18	> 20 HU and < 85 % pancreas density
PANCREATIC DUCTAL ADENOCARCINOMA	17	Histology
	65	

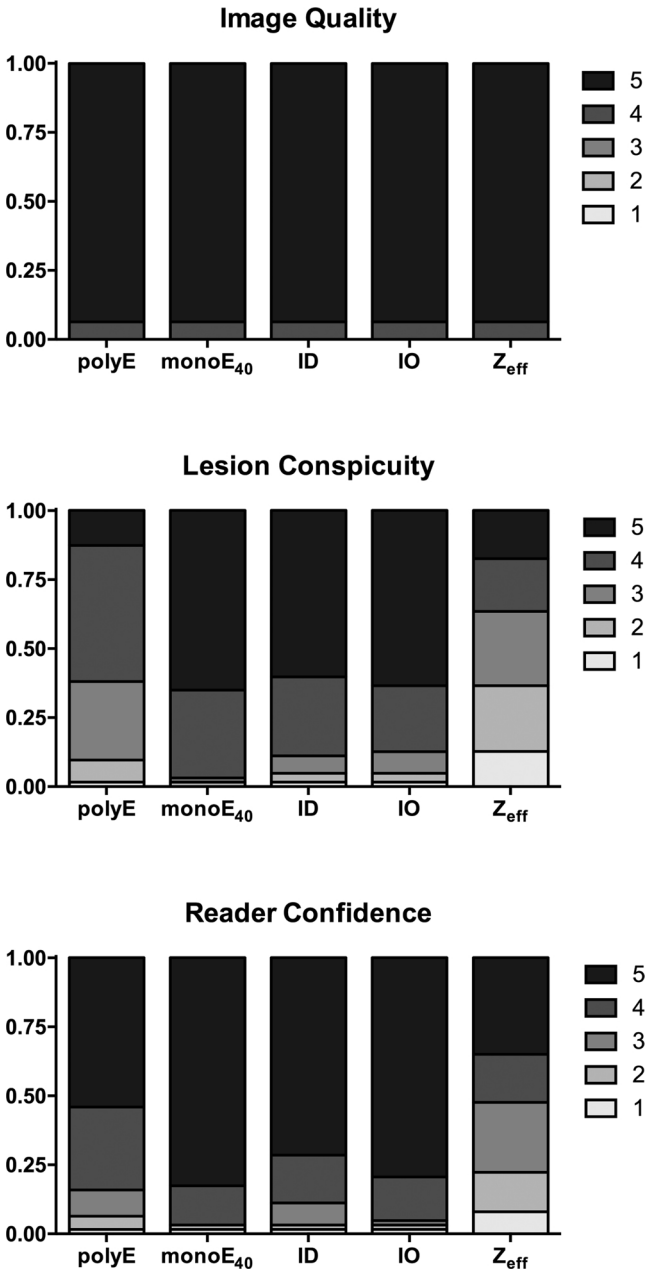

Fig. 1. Distribution of subjective Likert scores regarding image quality (top), lesion conspicuity (middle) and reader confidence (bottom). Except Zeff, all spectral reconstructions received significantly higher scores than polyenergetic images.

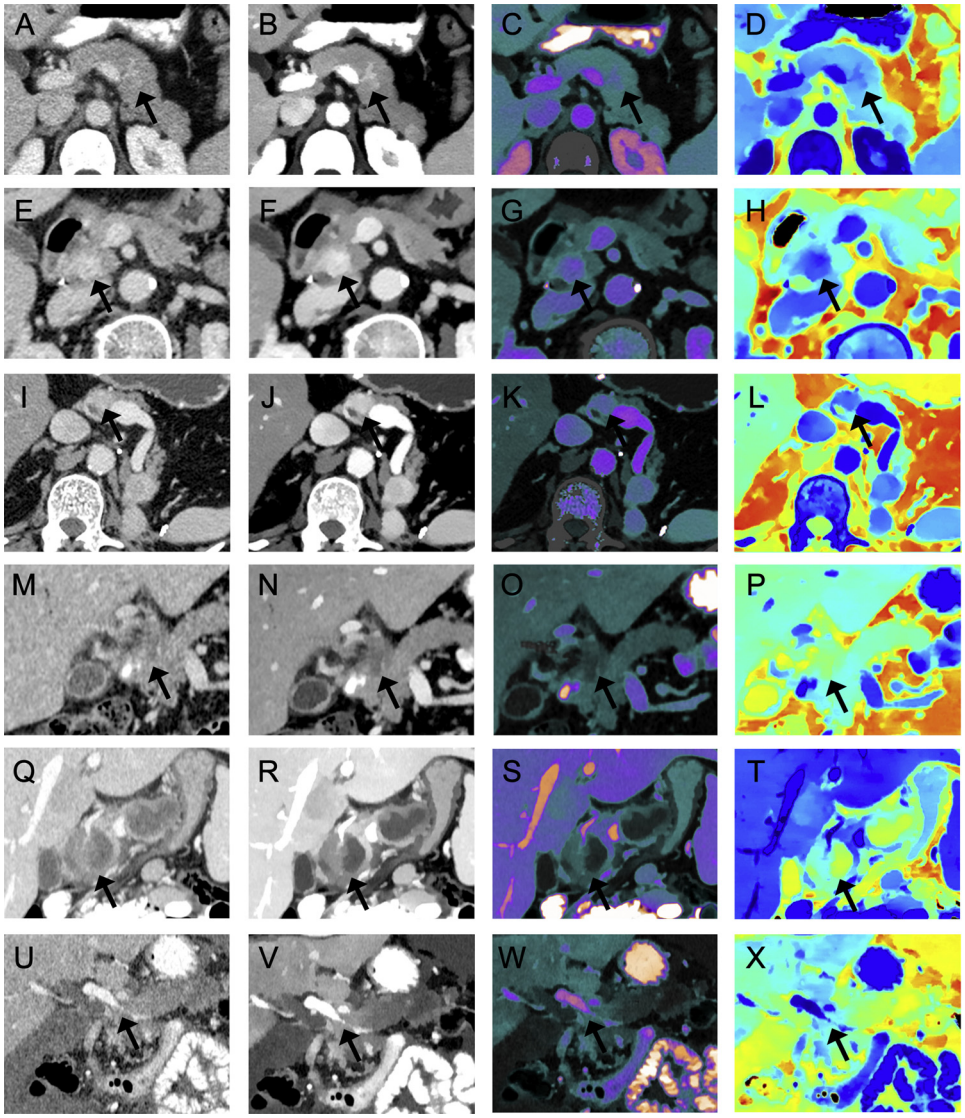

Fig. 2. Examples of polyenergetic images (left column), monoenergetic images at 40 keV (second from left column), iodine overlay images (second from right column) and Zeff reconstructions (right column). Arrows indicate improved visualization of pancreatic lesions (A-D: neuroendocrine tumor, E–H, I-L: metastasis, M–P, Q-T: PDAC) and tumor-related vessel compression (U–X).

and excellent with kappa values of 0.73-0.81 (Table 4). In summary, low keV monoE reconstructions as well as iodine maps provide subjectively significantly better lesion conspicuity and reader confidence compared to conventional polyE images.

3.3. Objective analysis

3.3.1. Contrast-to-noise ratio

PolyE images showed significantly lower CNR values compared to monoE images at 40 keV and 50 keV, no significant differences to monoE reconstructions of 60–80 keV, and higher CNR compared to monoE reconstructions above or equal to 90 keV (Fig. 3, Table 5).

Table 4
Inter-reader agreement in terms of subjective lesion conspicuity and reader confidence displayed as kappa values. polyE: polyenergetic reconstruction; monoE: monoenergetic reconstruction; ID: iodine density; IO: iodine overlay; Zeff: Z effective.

	polyE	monoE 40	ID	IO	Z_{eff}
Lesion Conspicuity	0.76	0.81	0.73	0.80	0.80
Reader Confidence	0.75	0.80	0.80	0.79	0.79

Table 3
Significance levels of subjective ratings regarding lesion conspicuity and reader confidence comparing conventional images and spectral reconstructions. polyE: polyenergetic reconstruction; monoE: monoenergetic reconstruction; ID: iodine density; IO: iodine overlay; Zeff: Z effective.

	polyE / monoE 40	polyE / ID	polyE / IO	polyE / Z_{eff}	monoE 40 / ID	monoE 40 / IO	monoE 40 / Z_{eff}	ID / IO	ID / Z_{eff}	IO / Z_{eff}
Lesion Conspicuity	< 0.0001*	< 0.0001*	< 0.0001*	0.0055*	0.4178	0.6010	< 0.0001*	0.8013	< 0.0001*	< 0.0001*
Reader Confidence	0.0005*	0.0555	0.0023*	0.0014*	0.1178	0.6423	< 0.0001*	0.2663	< 0.0001*	< 0.0001*

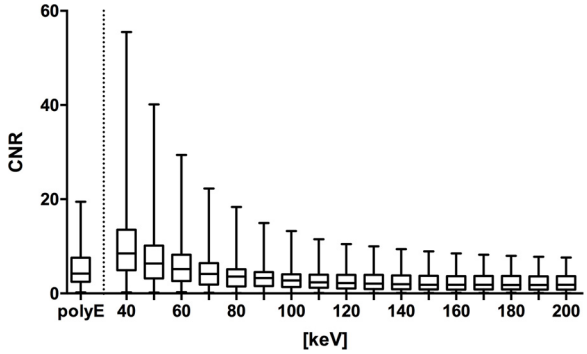

Fig. 3. CNR of pancreatic lesions to circumjacent organ parenchyma showing a stepwise increase with decreasing keV levels of monoenergetic images. Optimal CNR is provided at 40 keV.

Table 5
p- values comparing contrast-to-noise ratio at different monoenergetic reconstructions (monoE) with polyenergetic reconstruction (polyE) and monoenergetic reconstruction with 40 keV (monoE 40).

	PolyE	monoE 40
monoE 40	< 0.0001*	
monoE 50	0.0093*	0.0310*
monoE 60	0.3927	0.0001*
monoE 70	0.5256	< 0.0001*
monoE 80	0.0846	< 0.0001*
monoE 90	0.0084*	< 0.0001*
monoE 100	0.0010*	< 0.0001*
monoE 110	0.0002*	< 0.0001*
monoE 120	< 0.0001*	< 0.0001*
monoE 130	< 0.0001*	< 0.0001*
monoE 140	< 0.0001*	< 0.0001*
monoE 150	< 0.0001*	< 0.0001*
monoE 160	< 0.0001*	< 0.0001*
monoE 170	< 0.0001*	< 0.0001*
monoE 180	< 0.0001*	< 0.0001*
monoE 190	< 0.0001	< 0.0001
monoE 200	< 0.0001	< 0.0001

Similarly, monoE reconstructions with low keV revealed significantly higher CNR values compared to high keV reconstructions (Fig. 3, Table 5). To sum up, highest CNR values were achieved with low keV monoE reconstructions.

3.3.2. Monoparametric analysis

Monoparametric comparisons revealed significant differences between cystic lesions and all other groups for all parameters tested (Fig. 4A-E). The same results was found when comparing hyperdense lesions with PDAC and other hypodense lesions. PDAC and isodense lesions differed significantly only with respect to ID maps, polyE and $monoE_{60}$ images, while PDAC and other hypodense lesions showed significant differences in reconstructions for monoE > 70 keV, polyE and VNC images, but not ID maps and Z_{eff}. Good inter-observer agreement was reached for all parameters with R^2 between 0.77 and 0.90 (Fig. 5).

Despite statistically significant differences between the groups, marked overlap of the boxplots was observed, especially for the groups of hypodense and isodense lesions as well as PDAC. Normalization to the iodine contents of the celiac trunc could reduce this overlap slightly but did not change the overall result.

Variability could be reduced further by calculation of the ratios between the lesions and surrounding unaffected pancreatic tissue (l-p-ratio; Fig. 4F-*J*). PDAC and isodense lesions could be better discriminated using l-p-ratios compared to absolute values, with significant differences for all monoE reconstructions < 170 keV as well as all other parameters except VNC. Additional statistical significance was found between PDAC and hypodense lesions regarding $monoE_{70}$, with all other parameters reflecting the results of the absolute values. Still a distinct overlap of the boxplots was observed (Fig. 4F-*J*).

In summary, significant attenuation/iodine differences were primarily found between cystic vs. non-cystic lesions and hyperdense vs. hypodense lesions; all other lesion types exhibited considerable data overlap. Neither normalization to the injected iodine dose nor calculation of lesion-to-tissue ratios reduced data variability enough to overcome this limitation.

4. Discussion

DECT has already added several new parameters to the clinical portfolio [28–31] over the last years and has shown to be instrumental at the diagnostic assessment of pancreatic lesions [22,32–34]. In this study, we aimed to examine if these results could be confirmed for different spectral reconstructions acquired with a novel spectral detector CT scanner (SDCT) and to further investigate the diagnostic value of quantitative spectral parameters for pancreatic lesion characterization.

Subjective analyses revealed significantly enhanced lesion conspicuity and reader confidence using monoE images at low keV levels relative to polyE images which is in consequence of the increased attenuation of iodine at energy levels close to its absorption maximum (33 keV) [35,36]. Thus, small differences in iodine concentration are accentuated in low keV reconstructions, and lesions can be discriminated more accurately from their circumjacent tissue than in polyE images. A similar effect was seen in color-coded IO images. These results are substantiated by significantly higher CNR of low keV images compared to conventional polyE reconstructions. These findings are in accordance with previous studies using tube-based DECT [22, 32–34]. Low keV levels may especially offer advantages in detection of small lesions or lesions with only little contrast to the surrounding pancreatic tissue. Additionally, classification of a tumor as 'borderline resectable' may also potentially be facilitated. In select cases of incidentally detected pancreatic lesions, it might be feasible to omit additional dedicated pancreatic imaging protocols, if diagnostic confidence using spectral data of the initial routine scan obtained in portal venous phase is high enough; however, this has to be verified in a systematic evaluation comparing spectral reconstructions obtained from dedicated pancreatic phase CT and portal-venous phase CT. As spectral information is available for every scan at SDCT [23], such analyses can be carried out routinely and have become more frequently requested by referring physicians at our institution, especially in diagnostically challenging or clinically complex cases. Another important aspect resulting from the increased conspicuity in low keV monoE images is the possible reduction of radiation exposure or contrast media which have been discussed in previous studies [37–39].

Besides improved subjective visual impression, quantitative analysis of spectral parameters may help at the differentiation between pancreatic lesions of different types. In our study, all non-PDAC lesions proven by either histology, ultrasound, MRI or follow-up were assigned to four groups based on their HU values: cystic, hypodense, isodense or hyperdense (Fig. 4).

Although monoparametric analyses found significant differences between lesion groups, a marked overlap of absolute data was observed. Since most of the spectral parameters are based on the attenuation spectrum of iodine, measured values were normalized to the amount of iodine in the celiac trunc in order to eliminate variabilities due to differences in contrast agent injections. However, this did not lead to a significant change in the results, likely due to standardized injection procedures with little variations/deviations. Another approach consisted of the calculation of lesion-to-parenchyma ratios in order to underline differences in vascularization and perfusion between healthy tissue and pancreatic lesions. Indeed, these ratios reduced variability in the data and provided more robust statistical significances

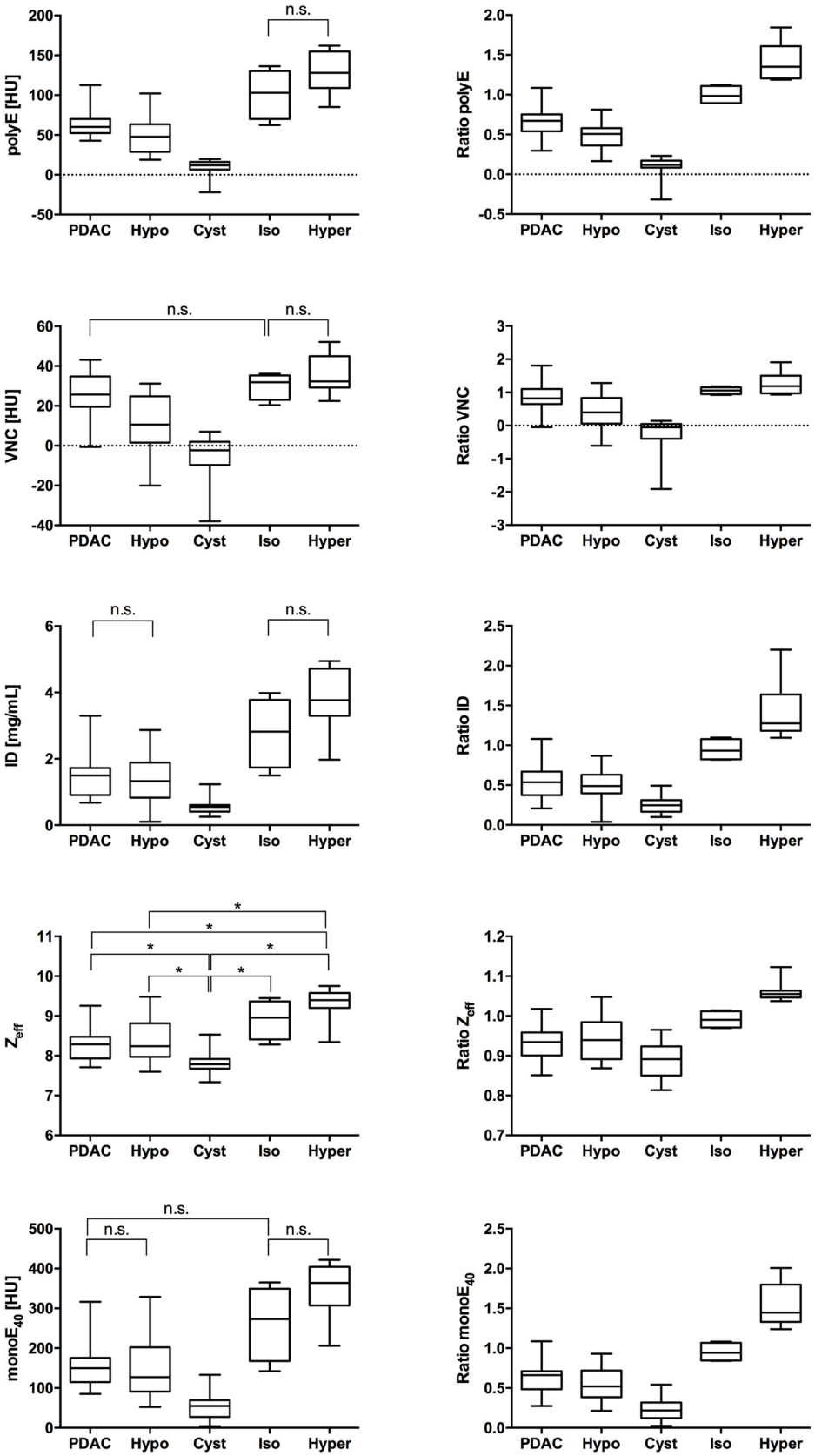

Fig. 4. Comparison of mean absolute CT numbers in polyenergetic images, VNC and monoE40 as well as iodine and Zeff values (left column) and the respective lesion-to-parenchyma ratios (right column) dependent on the lesion type. Asterix indicating statistically significant differences; n.s.: no statistical significance.

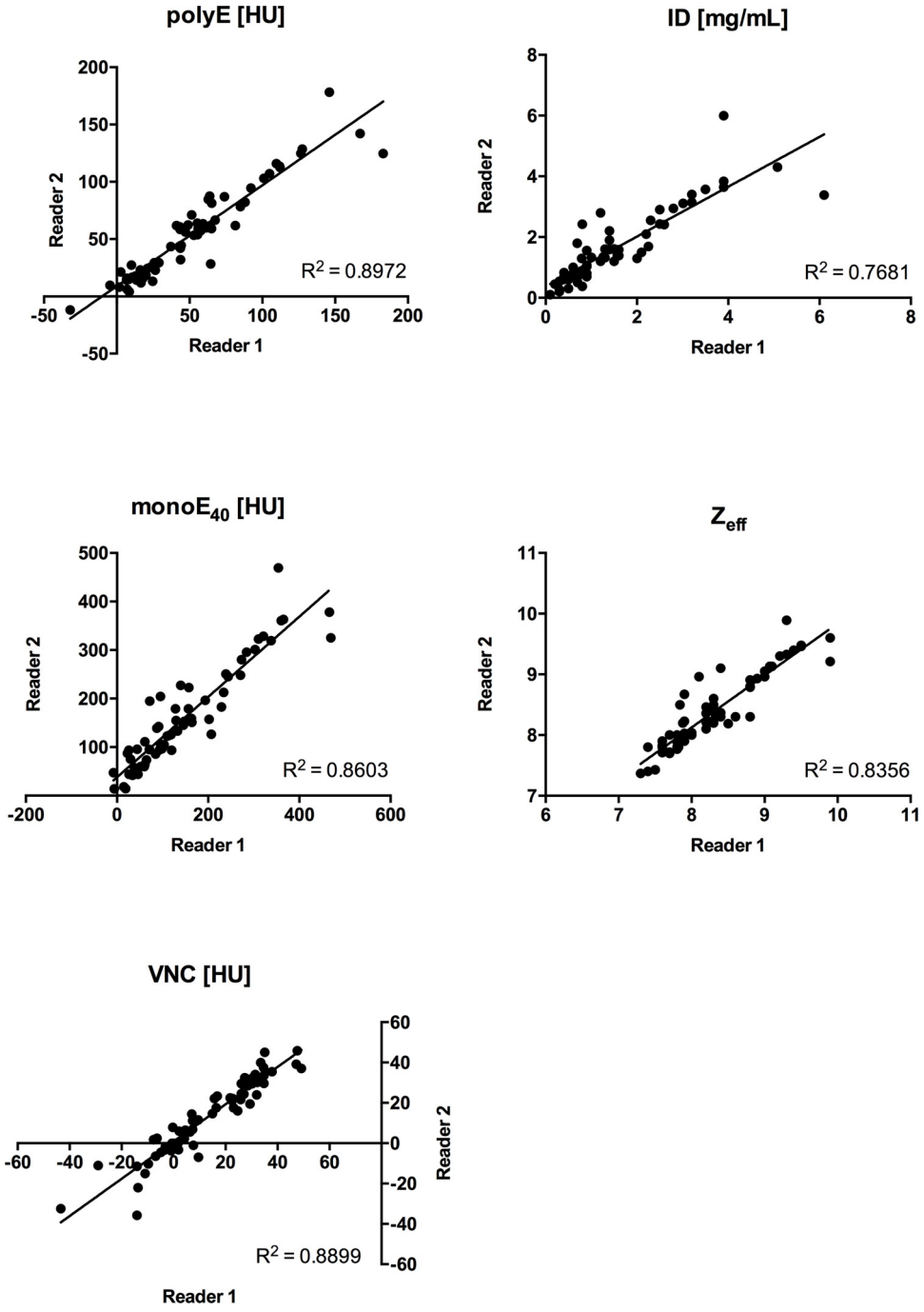

Fig. 5. Interreader agreement in ROI-based quantitative measurements of attenuation (polyE, monoE40, VNC), iodine and Zeff values.

between groups, which predestines them as a potentially more accurate parameter for lesion differentiation than absolute values. Yet, data overlap still did not allow for a confident discrimination between PDAC and other (especially hypodense) lesions.

Besides the retrospective nature of the study as well as the rather small number of patients previously alluded to, patient selection for this study may constitute a limitation since it was based on CT reports mentioning pancreatic lesions. In fact, only patients were included for which the respective lesions were already detected visually on the conventional polyE images. Therefore, results may not be applicable to smaller lesions or some low-contrast lesions. This may be reflected by the very small number of lesions (n = 4) allocated to the isodense lesion group. Second, due to the limited sample size, we did not assess diagnostic accuracy for pancreatic lesion detection. Third, owed to the various small lesion subgroups and the lack of histological information for the majority of non-PDAC lesions, the latter were clustered based on their HU values to facilitate a comprehensive quantitative comparison. Last, it is known that dedicated pancreatic phase CT offers superior lesion-to-parenchyma contrast compared to portal-venous phase [40,41]. However, we had to refrain from comparing spectral results obtained from these two phases as a considerable number of lesions was incidentally detected in routine staging scans solely comprising a portal-venous phase.

5. Conclusions

In conclusion, we found that the subjective analysis revealed a significant added value of SDCT-derived low keV monoE and iodine

overlay images with regards to lesion conspicuity and reader confidence which was substantiated by higher lesion-to-parenchyma ratios. Thus, these reconstructions should be considered for supplementary use in the clinical routine where possible.

6. Disclosures

David Maintz and Jan Borggrefe: received speakers' honoraria from Philips Healthcare. Simon Lennartz: received exemption from clinical duties for research outside this specific project as a part of a research agreement between Philips Healthcare and University Hospital Cologne; received travel cost reimbursement from Philips Healthcare.

Declaration of Competing Interest

The authors of this manuscript declare relationships with the following companies: David Maintz and Jan Borggrefe: received speakers' honoraria from Philips Healthcare. Simon Lennartz: received exemption from clinical duties for research outside this specific project as a part of a research agreement between Philips Healthcare and University Hospital Cologne; received travel cost reimbursement from Philips Healthcare.

Funding

This study has received funding by European Union Seventh Framework Programme (FP7/2007-2013) under Grant Agreement 603,028 (Image-Guided Pancreatic Cancer Therapy Project).

Role of the funding source

C.H. was partly excempted from clinical duties. Research contribution of S.E. was partly financed under the referring Grant Agreement.

Acknowledgments

The authors would like to thank Doaa Emara, MD for contribution to statistical analysis, and Annika Thillmann and Swetlana Weiss for technical support.

References

[1] R. Siegel, D. Naishadham, A. Jemal, Cancer statistics 2012, CA Cancer J. Clin. 62 (January-February (1)) (2012) 10–29.
[2] E.R. Witkowski, J.K. Smith, J.F. Tseng, Outcomes following resection of pancreatic cancer, J. Surg. Oncol. 107 (January (1)) (2013) 97–103.
[3] J. Klapman, M.P. Malafa, Early detection of pancreatic cancer: why, who, and how to screen, Cancer Control 15 (October (4)) (2008) 280–287.
[4] M.P. Callery, K.J. Chang, E.K. Fishman, et al., Pretreatment assessment of resectable and borderline resectable pancreatic cancer: expert consensus statement, Ann. Surg. Oncol. 16 (July (7)) (2009) 1727–1733.
[5] M. Bockhorn, F.G. Uzunoglu, M. Adham, et al., International Study Group of Pancreatic Surgery. Borderline resectable pancreatic cancer: a consensus statement by the International Study Group of Pancreatic Surgery (ISGPS), Surgery 155 (June (6)) (2014) 977–988.
[6] N.E. Lopez, C. Prendergast, A.M. Lowy, Borderline resectable pancreatic cancer: definitions and management, World J. Gastroenterol. 20 (August (31)) (2014) 10740–10751.
[7] R. Vargas, M. Nino-Murcia, W. Trueblood, et al., MDCT in Pancreatic adenocarcinoma: prediction of vascular invasion and resectability using a multiphasic technique with curved planar reformations, AJR Am. J. Roentgenol. 182 (2004) 419–425.
[8] D.V. Sahani, Z.K. Shah, O.A. Catalano, et al., Radiology of pancreatic adenocarcinoma: current status of imaging, J. Gastroenterol. Hepatol. 23 (January (1)) (2008) 23–33.
[9] E.P. Tamm, P.M. Silverman, C. Charnsangavej, et al., Diagnosis staging, and surveillance of pancreatic cancer, AJR Am. J. Roentgenol. 180 (May (5)) (2003) 1311–1323.
[10] Y.L. Bronstein, E.M. Loyer, H. Kaur, et al., Detection of small pancreatic tumors with multiphasic helical CT, AJR Am. J. Roentgenol. 182 (March (3)) (2004) 619–623.
[11] R.W. Prokesch, L.C. Chow, C.F. Beaulieu, et al., Isoattenuating pancreatic adenocarcinoma at multi-detector row CT: secondary signs, Radiology 224 (September (3)) (2002) 764–768.
[12] J.M. Winter, J.L. Cameron, K.D. Lillemoe, et al., Periampullary and pancreatic incidentaloma: a single institution's experience with an increasingly common diagnosis, Ann. Surg. 243 (2006) 673–680 discussion 80-3.
[13] W. Kimura, H. Nagai, A. Kuroda, et al., Analysis of small cystic lesions of the pancreas, Int. J. Pancreatol. 18 (1995) 197–206.
[14] K.S. Spinelli, T.E. Fromwiller, R.A. Daniel, et al., Cystic pancreatic neoplasms: observe or operate, Ann. Surg. 239 (2004) 651–657 discussion 7-9.
[15] S. Edirimanne, S.J. Connor, Incidental pancreatic cystic lesions, World J. Surg. 32 (2008) 2028–2037.
[16] M. Patino, A. Prochowski, M.D. Agrawal, et al., Material separation using dual-energy CT: current and merging applications, Radiographics. 36 (July-August (4)) (2016) 1087–1105.
[17] N. Rassouli, M. Etesami, A. Dhanantwari, et al., Detector-based spectral CT with a novel dual-layer technology: principles and applications, Insights Imaging 8 (December (6)) (2017) 589–598.
[18] R.E. Alvarez, A. Macovski, Energy-selective reconstructions in X-ray computerized tomography, Phys. Med. Biol. 21 (1976) 733–744.
[19] S. Aran, K.W. Shaqdan, H.H. Abujudeh, Dual-energy computed tomography (DECT) in emergency radiology: basic principles, techniques, and limitations, Emerg. Radiol. 21 (August (4)) (2014) 391–405.
[20] H.W. Goo, J.M. Goo, Dual-energy CT: new horizon in medical imaging, Korean J. Radiol. 18 (July-August (4)) (2017) 555–569.
[21] B. Quiney, A. Harris, P. McLaughlin, et al., Dual-energy CT increases reader confidence in the detection and diagnosis of hypoattenuating pancreatic lesions, Abdom. Imaging 40 (April (4)) (2015) 859–864.
[22] P. Bhosale, O. Le, A. Balachandran, et al., Quantitative and qualitative comparison of single-source dual-energy computed tomography and 120-kVp computed tomography for the assessment of pancreatic ductal adenocarcinoma, J. Comput. Assist. Tomogr. 39 (November-December (6)) (2015) 907–913.
[23] The clinical impact of retrospective analysis in spectral detector dual energy body CT, in: M. Gabbai, I. Leichter, R. Zimam (Eds.), Radiological Society of North America 2013 Scientific Assembly and Annual Meeting, 2013.
[24] T. Johnson, C. Fink, S.O. Schoenberg, et al., Dual Energy CT in Clinical Practice, (2011) ISBN: 978-3-642-26590-7.
[25] P.M. Carrascosa, R.C. Cury, M.J. García, et al., Dual-Energy CT in Cardiovascular Imaging, (2015) ISBN: 978-3-319-21226-5.
[26] S. Haneder, F. Siedek, J. Doerner, et al., Thoracic-abdominal imaging with a novel dual-layer spectral detector CT: intra-individual comparison of image quality and radiation dose with 128-row single-energy acquisition, Acta radiol. 1 (January) (2018) 284185118762611.
[27] Y. Yamada, M. Jinzaki, T. Hosokawa, et al., Abdominal CT: an intra-individual comparison between virtual monochromatic spectral and polychromatic 120-kVp images obtained during the same examination, Eur. J. Radiol. 83 (October (10)) (2014) 1715–1722.
[28] M.J. Kang, C.M. Park, C.H. Lee, et al., Dual-energy CT: clinical applications in various pulmonary diseases, Radiographics 30 (May (3)) (2010) 685–698.
[29] S. Aran, L. Daftari Besheli, M. Karcaaltincaba, et al., Applications of dual-energy CT in emergency radiology, AJR Am. J. Roentgenol. 202 (April (4)) (2014) W314–24.
[30] M.D. Agrawal, D.F. Pinho, N.M. Kulkarni, et al., Oncologic applications of dual-energy CT in the abdomen, Radiographics 34 (May-June (3)) (2014) 589–612.
[31] D. Simons, M. Kachelriess, H.P. Schlemmer, Recent developments of dual-energy CT in oncology, Eur. Radiol. 24 (April (4)) (2014) 930–939.
[32] B.N. Patel, J.V. Thomas, M.E. Lockhart, et al., Single-source dual-energy spectral multidetector CT of pancreatic adenocarcinoma: optimization of energy level viewing significantly increases lesion contrast, Clin. Radiol. 68 (February (2)) (2013) 148–154.
[33] M.M. McNamara, M.D. Little, L.F. Alexander, et al., Multireader evaluation of lesion conspicuity in small pancreatic adenocarcinomas: complimentary value of iodine material density and low keV simulated monoenergetic images using multiphasic rapid kVp-switching dual energy CT, Abdom. Imaging 40 (June (5)) (2015) 1230–1240.
[34] L.D. Di Maso, J. Huang, M.F. Bassetti, et al., Investigating a novel split-filter dual-energy CT technique for improving pancreas tumor visibility forradiation therapy, J. Appl. Clin. Med. Phys. 19 (September (5)) (2018) 676–683.
[35] C.H. McCollough, S. Leng, L. Yu, et al., Dual- and multi-energy CT: principles, technical approaches, and clinical applications, Radiology. 276 (September (3)) (2015) 637–653.
[36] C.A. Coursey, R.C. Nelson, D.T. Boll, et al., Dual-energy multidetector CT: how does it work, what can it tell us, and when can we use it in abdominopelvic imaging? Radiographics 30 (July-August (4)) (2010) 1037–1055.
[37] W. Stiller, C.B. Schwarzwaelder, C.M. Sommer, S. Veloza, B.A. Radeleff, H.U. Kauczor, Dual-energy, standard and low-kVp contrast-enhanced CT-cholangiography: a comparative analysis of image quality and radiation exposure, Eur. J. Radiol. 81 (2012) 1405–1412.
[38] R.W. van Hamersvelt, N.G. Eijsvoogel, C. Mihl, et al., Contrast agent concentration optimization in CTA using low tube voltage and dual-energy CT in multiple vendors: a phantom study, Int. J. Cardiovasc. Imaging 34 (2018) 1265.
[39] J.R. Grajo, D.V. Sahani, Dual-energy CT of the abdomen and pelvis: radiation dose considerations, J. Am. Coll. Radiol. 15 (8) (2018) 1128–1132.
[40] J.G. Fletcher, M.J. Wiersema, M.A. Farrell, et al., Pancreatic malignancy: value of arterial, pancreatic, and hepatic phase imaging with multi-detector row CT, Radiology 229 (2003) 81–90.
[41] D.S. Lu, S. Vedantham, R.M. Krasny, B. Kadell, W.L. Berger, H.A. Reber, Two-phase helical CT for pancreatic tumors: pancreatic versus hepatic phase enhancement of tumor, pancreas, and vascular structures, Radiology 199 (1996) 697–701.